LOW TRANSVERSE MOMENTUM HADRON-NUCLEUS INTERACTIONS AT HIGH ENERGY*

By C. Halliwell

University of Illinois at Chicago Circle**

and

Massachusetts Institute of Technology

(Received August 19, 1980)

Implications of a new experiment on our understanding of hadron-nucleus interactions are discussed.

PACS numbers: 13.85.—t

Hadron-nucleus (hA) interactions have been studied extensively in recent years [1]. For incoherent interactions, it has been shown that the total multiplicity of charged secondaries does not depend strongly on atomic number, A, or on the incident particle type [2]. For the most energetic secondaries, there is a slight depletion in their production when hA interactions are compared to hadron–nucleon (hN) interactions [3]. The mechanism by which newly formed secondaries (or their constituents) lose energy in, or interact with, nuclear matter is of fundamental interest. The contents of this report will be a discussion of various aspects of such hA interactions.

This report will be divided into five sections. In Section 1 a review of some of the reasons for studying hA interactions will be given. In Section 2 previous experimental facts and their interpretation will be presented. Only data relevant to the understanding of the new data to be prsesented in this paper will be dealt with. This will be followed in Section 3 by a description of an hA experiment that has been carried out at Fermilab. The data that resulted from this experiment will be presented in Section 4. This data will then be compared with various theoretical models in Section 5 followed by general conclusions in Section 6.

---

* Presented at the XX Cracow School of Theoretical Physics, Zakopane, May 29 — June 11, 1980.

** Address: Physics Department, University of Illinois at Chicago Circle, Box 4348, Chicago, IL 60680, USA.

1. Estimation of the interaction time of a hadron-nucleon collision

Consider an hN interaction as shown in Fig. 1. The incident hadron has total energy E, 3-momentum $\vec{p}$ and rest mass m. Similarly, the produced hadronic state, h', is described by E', $\vec{p}'$, and m'. (The hadronic state discussed here need not be a single particle. It will, in general, eventually consist of many particles whose total invariant mass will be m'.) In order to make an estimate of the interaction time, consider the upper vertex in Fig. 1.

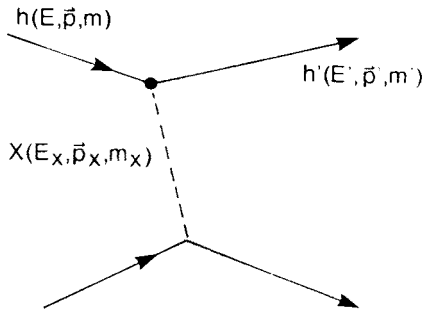

Fig. 1. The interaction hN → h'X. E, $\vec{p}$ and m are the total energy, 3-momentum and invariant mass respectively of the incident hadron, h. E', $\vec{p}'$ and m' are corresponding quantities of the produced hadronic state, h'

This vertex can be analyzed using the uncertainty principle. Assume momentum is conserved at this vertex and the exchanged particle, X, has a real rest mass m_X. An estimate of the lifetime of X (and therefore the time to produce the state h') is given by:

$$\tau \sim \frac{2E_X}{Q^2 - m_X^2}, \tag{1}$$

where E_X is the energy of the exchanged particle and Q^2 is given by:

$$Q^2 = (m^2 - m'^2/x)(1-x) - p_t^2(1+1/x), \tag{2}$$

$x = E'/E$ and p_t is the transverse momentum of X.

For the production of high momentum particles ($x \to 1$), the expression for the production time becomes:

$$\tau \sim \frac{2E_X}{m_X^2 + 2p_t^2}. \tag{3}$$

The basic form of equation (3) can be alternatively derived by just considering the fundamental interaction time in the hN center-of-mass frame. This will be $\sim 1/m_X$. Applying a time dilation factor of E_X/m_X results approximately in equation (3).

The distance travelled by h' (in the direction of the incident hadron) during τ is approximately:

$$l_z = \left(\frac{p'}{E'}\right)\tau. \tag{4}$$

Similarly, the transverse distance travelled by h′ is given by:

$$l_t = \left(\frac{p_t}{E'}\right)\tau. \tag{5}$$

For a small value of m_X expressions (4) and (5) become

$$l_z \sim \frac{E_X}{p_t^2} = \frac{(1-x)E}{p_t^2} \tag{6}$$

and

$$l_t \sim \frac{1-x}{xp_t}. \tag{7}$$

Typically, l_z is many fermis whereas l_t is of the order of one fermi. For example, for $E = 100$ GeV, $x = 0.7$ and $p_t = 0.3$ GeV/c, $l_z \sim 60$ fm. Consequently, low p_t interactions occur over large longitudinal distances compared to internucleon separations in nuclei.

The properties of the hadronic state that is produced immediately after an hN interaction cannot be studied directly in hN interactions; only indirect knowledge can be obtained by studying the properties of the asymptotic states, that is, the detected secondaries. However, by allowing the hadronic state to interfere with other nucleons soon after it is formed, it should be possible to study some of the state's properties. It is this fact that makes the study of hA interactions so interesting to pursue.

2. Summary of previous knowledge

In this section, facts that are relevant to understanding the new experimental data that is to be presented in Section 4 will be reviewed. No attempt will be made to present a comprehensive review of the extensive data from the many experiments that have studied hA interactions.

Previous hA experiments [1] have shown that at high energies the multiplication of hadrons within a nucleus is relatively weak. This is reflected in the observation that, with increasing nuclear thickness, there is at most a linear increase in the multiplicity of the produced hadrons [4]. This is shown in Fig. 2. It can be seen that proton-induced and pion-induced interactions both produce linear dependences. However, the rate of increase is different.

In an attempt to understand the origin of the different slopes the mean multiplicity, $\langle n \rangle_{hA}$, can be plotted against an alternative variable, $\bar{\nu}$, rather than the atomic number. $\bar{\nu}$ is a measure of the average amount of nuclear material involved in an inelastic hA interaction. The parameter $\bar{\nu}$ is given by [1]:

$$\bar{\nu} = \frac{A\sigma^{hN}}{\sigma^{hA}}, \tag{8}$$

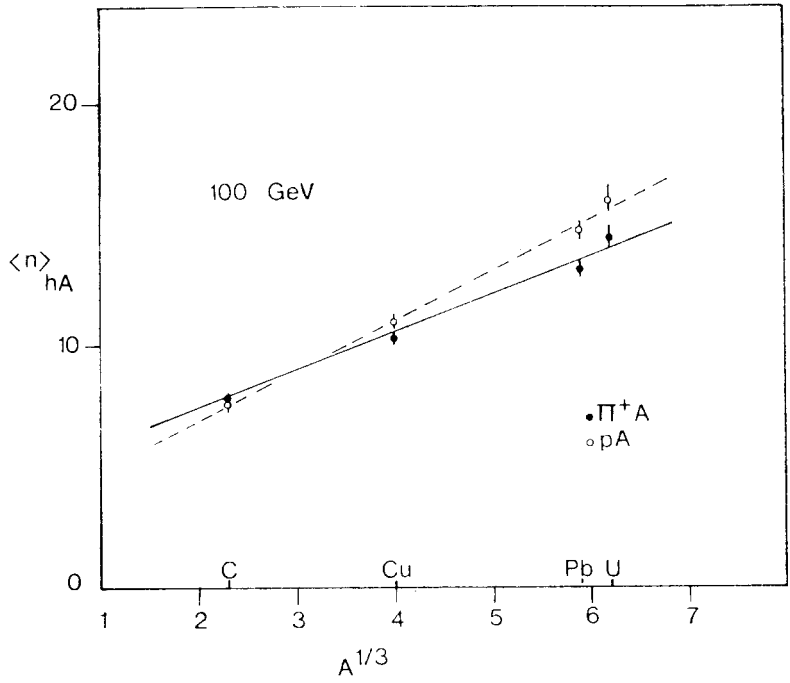

Fig. 2. The multiplicity of relativistic ($\beta \gtrsim 0.85$) secondaries vs. nuclear thickness, $A^{1/3}$. A is the atomic number of the target mucleus. The data are from Ref. [4]

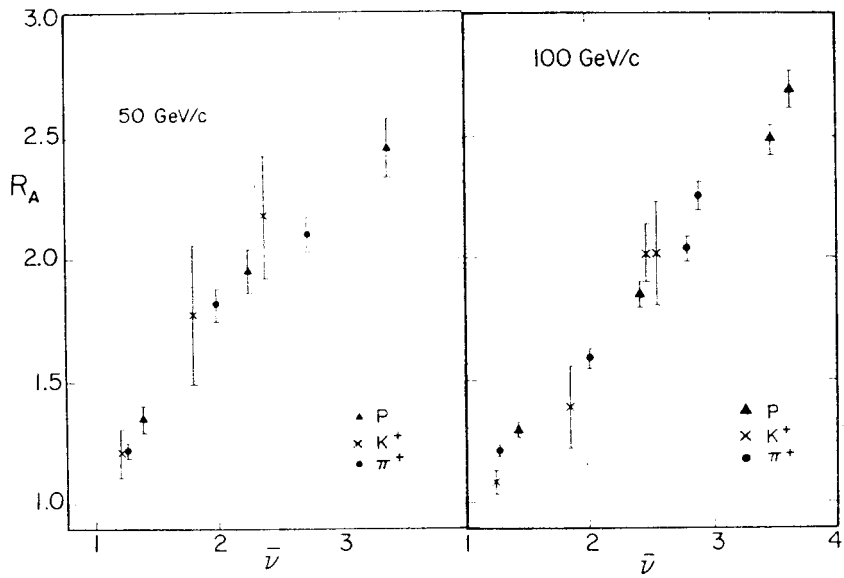

Fig. 3. Scaled multiplicity $R = \langle n \rangle_{hA}/\langle n \rangle_{hN}$ vs nuclear thickness as measured in terms of $\bar{\nu}$. Data are from Ref. [4]

where σ^{hN} is the hN absorption cross section and σ^{hA} is the corresponding hA cross section. Thus $\bar{\nu}$ is the average number of inelastic collisions that the incident hadron, h, would undergo in traversing the nucleus, A, assuming that all the collisions were governed by the incident hadron. It is emphasized that $\bar{\nu}$ depends not only on the type of nucleus being considered but also on the incident hadron.

One further modification in the presentation of the data can be performed. To eliminate the effects of different hN multiplicities ($\langle n\rangle_{hN}$) the hA multiplicities can be scaled with respect to $\langle n\rangle_{hN}$. The resulting variable, $R_A = \langle n\rangle_{hA}/\langle n\rangle_{hN}$ is shown in Fig. 3 plotted against $\bar{\nu}$ [5]. It is apparent that the effect of the incident hadron's identity is entirely accommodated by the use of the variable $\bar{\nu}$. The hypothesis that all collisions, other than the first, are governed by the cross section of a pion rather than that of the incident hadron can be examined with the use of the parameter $\bar{\nu}'$ [5]. The values of $\bar{\nu}'$ are given by the formula:

$$\bar{\nu}' = 1+(\bar{\nu}-1)\frac{\sigma^{\pi p}}{\sigma^{hp}}.$$

The multiplicity ratio R_A is plotted versus $\bar{\nu}'$ in Fig. 4. The universal behavior is no longer evident.

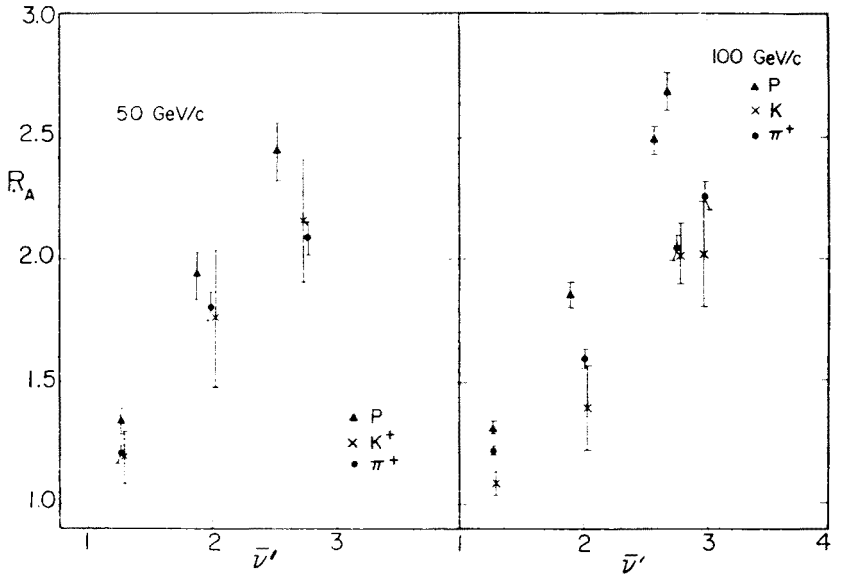

Fig. 4. Scaled multiplicity $R = \langle n\rangle_{hA}/\langle n\rangle_{hN}$ vs nuclear thickness as measured in terms of $\bar{\nu}'$. Data are from Ref. [4]

In summary, the idea that the hadronic state formed immediately after an hN interaction will undergo numerous collisions in a nucleus (with a probability governed by the identity of the incident hadron) will be used extensively in interpreting the data presented in Section 4.

3. *FNAL experiment #451*

An experiment has been performed [6] to study the inclusive process h + A → h′+ anything where h was either π^+, K^+ or p; h′ was either $\pi^\pm$, $K^\pm$, p or $\bar{p}$ and A, the nuclear target was either C, Al, Cu, Ag or Pb. The experimental apparatus consisted of the Fermilab M6E beam line and the Single Arm Spectrometer facility. An incident beam momentum (p_{inc}) of 100 GeV/c was used. The production of the fast secondary h′, was measured over a Feynman x range of $0.3 < x < 0.88$ [7] and a transverse momentum range of $0.18 < p_t < 0.5$ GeV/c. Data were taken simultaneously for the nine reaction types ($\pi\pi$, πK,πp, etc.) The details of the instrumentation of the beam line and the spectrometer have been summarized elsewhere [8]. Good $\pi-K-p$ separation was achieved over the entire kinematic range using the eight Cerenkov counters of the facility. A list of the targets used in the experiment is given in Table I and a summary of the kinematic points studied is given in Table II.

In a manner similar to that described in Ref. [8], the interaction rates were corrected for particle absorption and decay in the spectrometer, finite target thickness, multiple

TABLE I

Targets used in this experiment. Most data was taken with thick targets; other were used for finite thickness correction

Target	A	Thickness (g · cm^{-2})
C	12.0	1.37
		3.93
		5.79
Al	27.0	5.99
Cu	63.5	2.89
		5.94
		9.94
Ag	107.9	6.71
Pb	207.2	2.06
		4.00
		7.38

TABLE II

Summary of data runs. + signifies positive secondary in spectrometer; − signifies negative secondary in spectrometer

		x						
		.3	.4	.5	.6	.7	.8	.88
p_t	0.18			−				
	0.3	±	±	±	±	±	±	±
	0.5	±		±			±	

scattering losses in the spectrometer, particle misidentification and track reconstruction inefficiencies. The corrected rates were then used to obtain, for every channel, the invariant differential cross section $Ed^3\sigma/dp^3$(mb/GeV^2 per nucleus).

Previous measurements of the A-dependence of inclusive processes in the beam fragmentation region have been performed [9]. However, this experiment has the advantage that it was the continuation of an extensive study of the production of particles in hN collisions. [8] Consequently, many systematic effects that are present in comparing hA data with hN data from a different experiment were eliminated.

4. Experimental data from FNAL experiment #451

The most significant features of the data are shown in Figs. 5 and 6. In these figures the manner in which the differential cross section per nucleon depends on x, p_t and A is illustrated. The errors indicated are statistical. The overall normalization uncertainty is estimated to be 10%. The systematic uncertainty due to particle misidentification in the reactions with an outgoing kaon is less than 5%. The results shown are for channels with the highest statistics. The other channels exhibit similar trends.

The following general trends in the data should be noted:

1. Over the entire range of x covered in this experiment, the "effectiveness" of nucleons in the nucleus in producing particles decreases with A. This is true not only for channels where the outgoing particle is identical to the incoming one ($\pi^+ \to \pi^+$, $K^+ \to K^+$ and $p \to p$), but also for channels where the outgoing particle is different (e.g. $p \to \pi^+$).

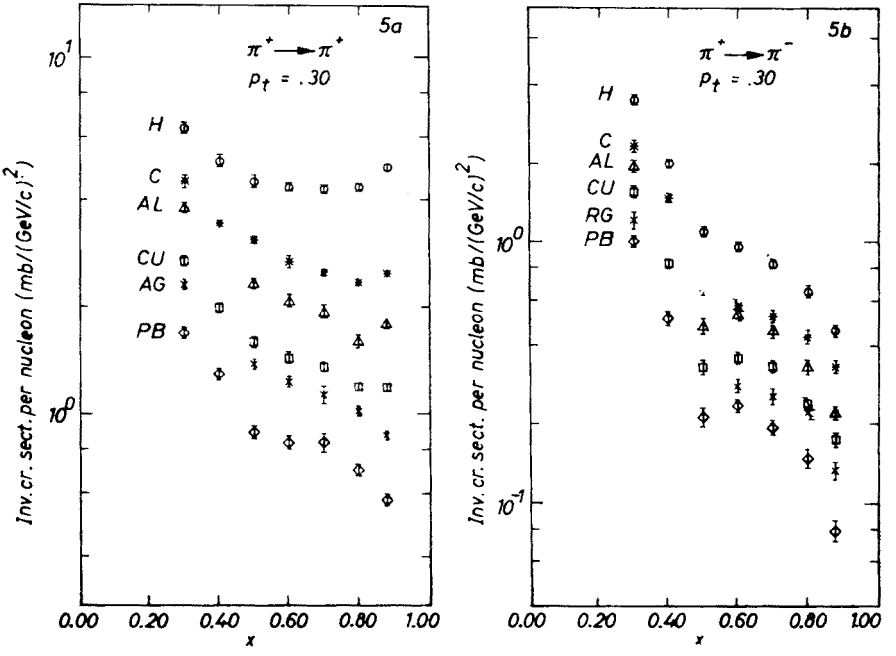

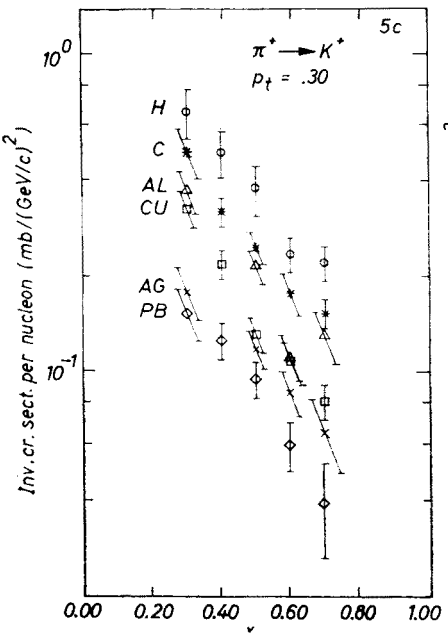
5c
$\pi^+ \rightarrow K^+$
p_t = .30
H
C
AL
CU
AG
PB
Inv. cr. sect. per nucleon (mb/(GeV/c)^2)
10^0
10^{-1}
0.00 0.20 0.40 0.60 0.80 1.00
v

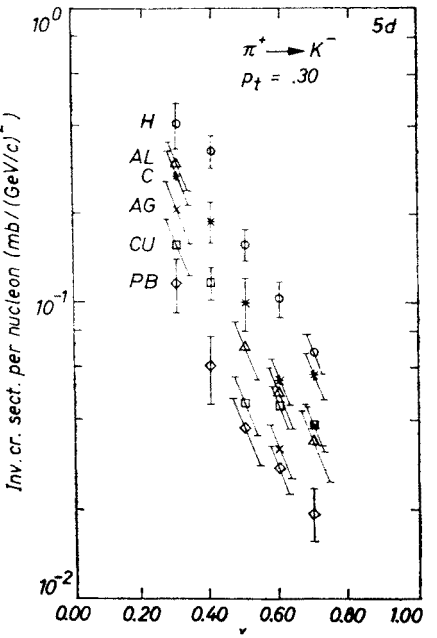
5d
$\pi^+ \rightarrow K^-$
p_t = .30
H
AL
C
AG
CU
PB
Inv. cr. sect. per nucleon (mb/(GeV/c)^2)
10^0
10^{-1}
10^{-2}
0.00 0.20 0.40 0.60 0.80 1.00
v

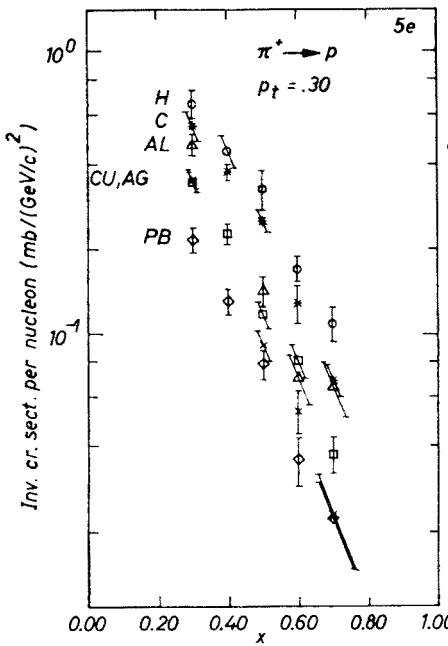
5e
$\pi^+ \rightarrow p$
p_t = .30
H
C
AL
CU,AG
PB
Inv. cr. sect. per nucleon (mb/(GeV/c)^2)
10^0
10^{-1}
0.00 0.20 0.40 0.60 0.80 1.00
x

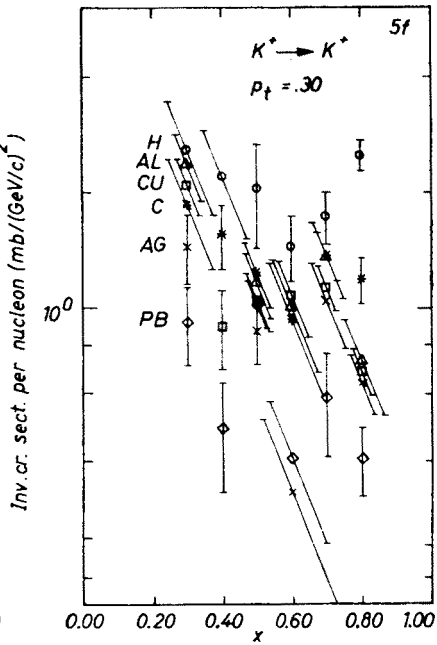
5f
$K^+ \rightarrow K^+$
p_t = .30
H
AL
CU
C
AG
PB
Inv. cr. sect. per nucleon (mb/(GeV/c)^2)
10^0
0.00 0.20 0.40 0.60 0.80 1.00
x

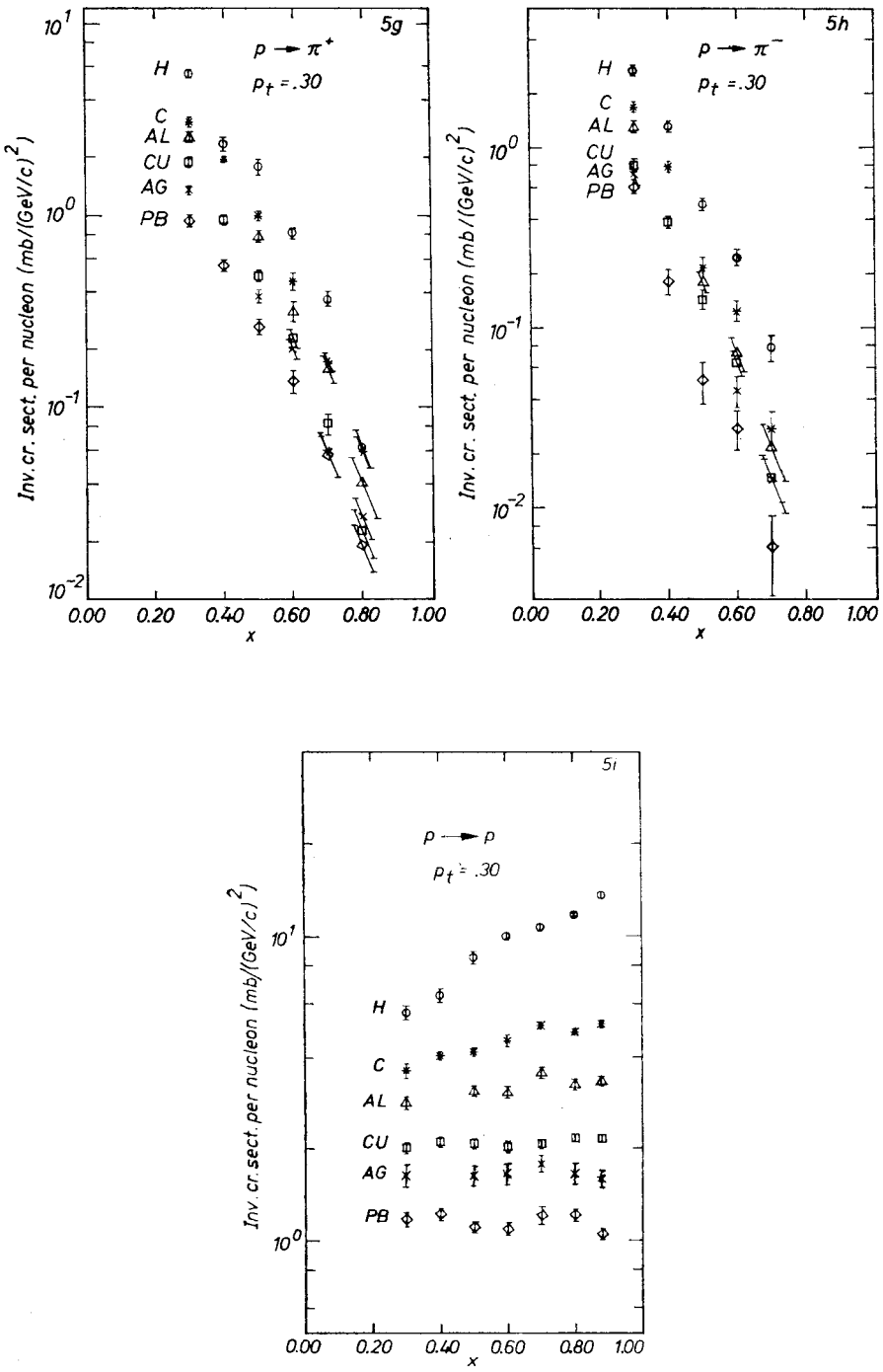

Fig. 5. The invariant differential cross section per nucleon vs Feynman x measured at $p_t = 0.3$ GeV/c. The hydrogen target data are from Ref. [8]

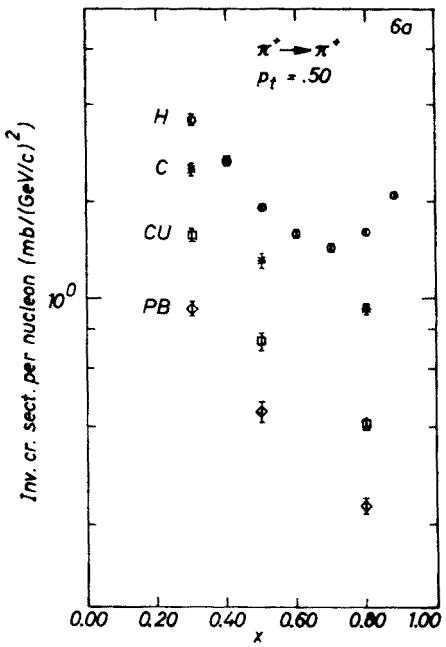
6a
$\pi^+ \rightarrow \pi^+$
$p_t = .50$
H
C
CU
PB
10^0
Inv. cr. sect. per nucleon $(mb/(GeV/c)^2)$
0.00 0.20 0.40 0.60 0.80 1.00
x

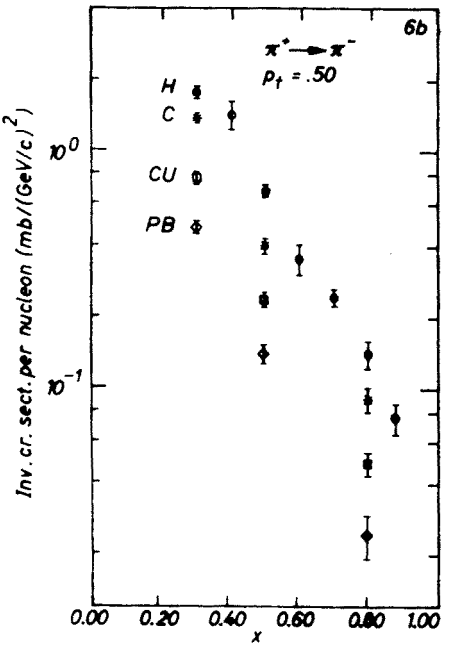
6b
$\pi^+ \rightarrow \pi^-$
$p_t = .50$
H
C
CU
PB
10^0
10^{-1}
Inv. cr. sect. per nucleon $(mb/(GeV/c)^2)$
0.00 0.20 0.40 0.60 0.80 1.00
x

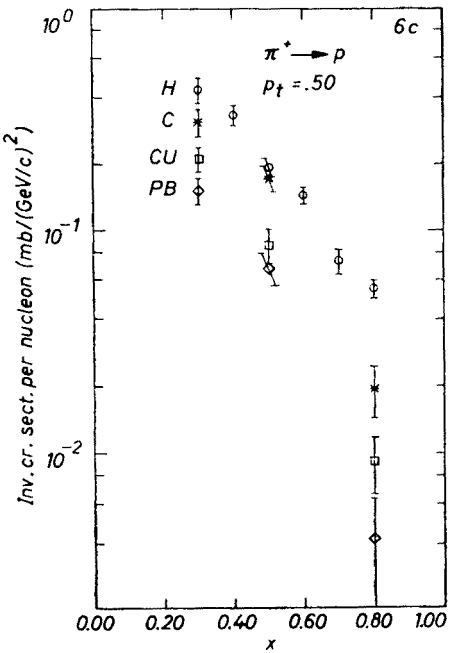
6c
$\pi^+ \rightarrow p$
$p_t = .50$
H
C
CU
PB
10^0
10^{-1}
10^{-2}
Inv. cr. sect. per nucleon $(mb/(GeV/c)^2)$
0.00 0.20 0.40 0.60 0.80 1.00
x

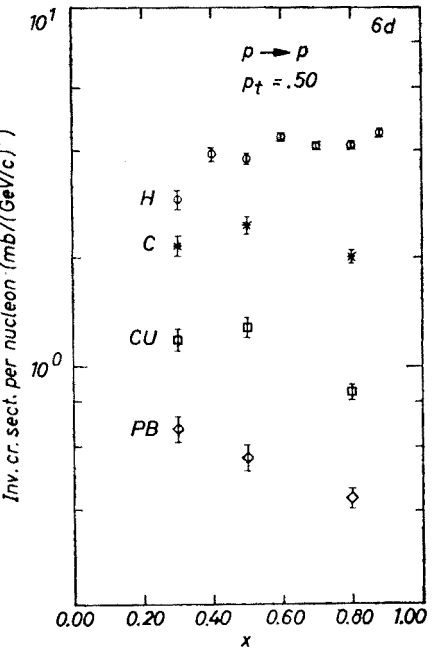
6d
$p \rightarrow p$
$p_t = .50$
H
C
CU
PB
10^1
10^0
Inv. cr. sect. per nucleon $(mb/(GeV/c)^2)$
0.00 0.20 0.40 0.60 0.80 1.00
x

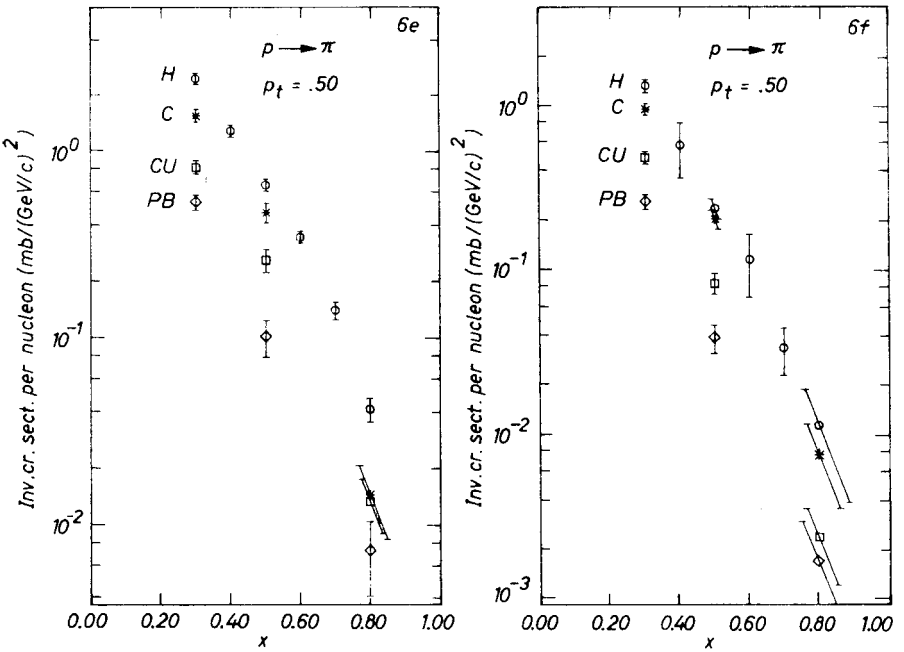

Fig. 6. The invariant differential cross section per nucleon vs Feynman x measured at $p_t = 0.5$ GeV/c. The hydrogen target data are from Ref. [8]

2. A further suppression in production of higher momentum secondaries occurs in certain channels (e.g. $\pi^+ \to \pi^+$ and $p \to p$).
3. In the $\pi \to \pi$ channel (in particular $\pi^+ \to \pi^-$), there is an enhancement at high x which has only a weak A dependence. A similar enhancement has been observed previously in hN interactions [10]. A possible interpretation in this case is that many of the high x pions originate from the decay of resonances coherently produced from the nucleus.

Relative production rates are shown in Fig. 7 for protons incident on a lead target. For comparison, corresponding data from hydrogen [8] are also shown. Although the production rates per nucleon from a lead target differ greatly from that of hydrogen, the relative rates appear to be the same.

To facilitate the presentation of all these data, the A dependence of the cross sections was fitted to the empirical form:

$$E\frac{d^3\sigma}{dp^3}(x, p_t, A) = \sigma_0(x, p_t)A^{\alpha(x,p_t)}, \tag{9}$$

where σ_0 and α are constants. A typical set od fata is shown in Fig. 8. The solid line is a fit to the *nuclear* ($A > 1$) data using equation (9). (It can be seen that this fit does not extrapolate to the measured hN data. This property of nuclear data has been seen previously in several experiments [11]. Conclusions drawn from experiments that use only one nuclear target in conjunction with hydrogen should therefore be treated with caution.)

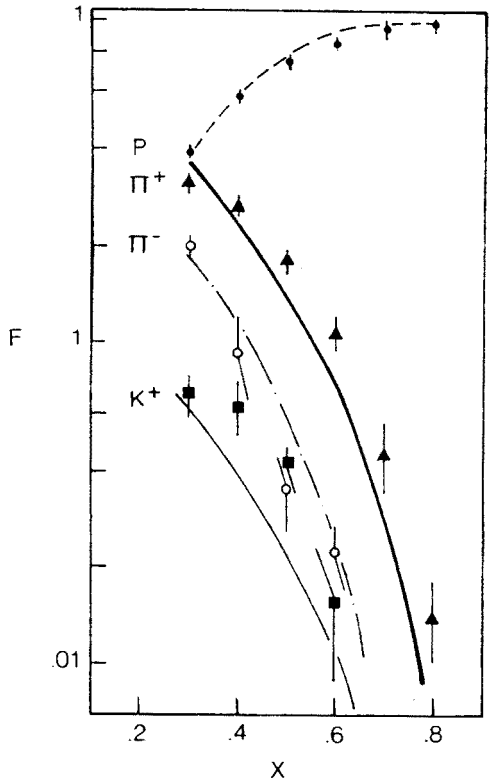

Fig. 7. Relative production rates for protons incident on a lead (points) and hydrogen target (lines). Hydrogen data are from Ref. [8]

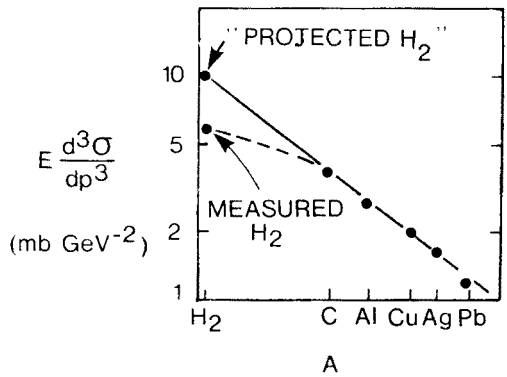

Fig. 8. Variation of the invariant differential cross section with atomic number. Data from the channel pA → pX is shown. The data were obtained at the kinematical point $x = 0.3$, $p_t = 0.3$ GeV/c. The line is a fit to the empirical form given in expression (9) in the main text

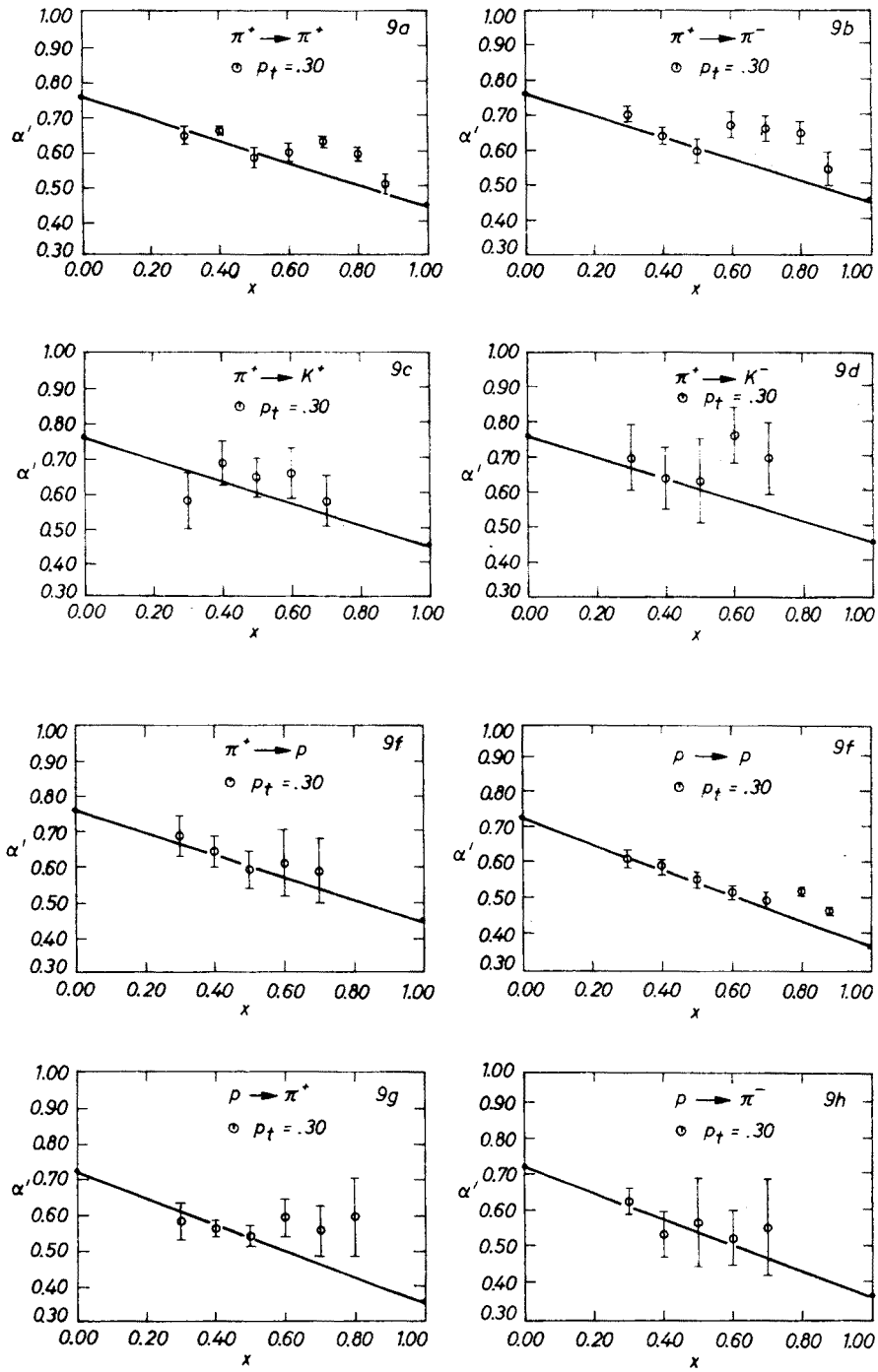

Fig. 9. The power $\alpha'(x)$ (listed in Table III) obtained from fits to the invariant differential cross section (per nucleus)

TABLE III

Results of fits: $E\frac{d^3\sigma_A}{dp^3} = \sigma_0 A^{\alpha'}$ and measured hydrogen cross section, $\sigma_H = E\frac{d^3\sigma_H}{dp^3}$

Reaction	x	α'	σ_0	σ_H
			[mb/(GeV/c)^2]	
$\pi^+ \to \pi^+$	.30	.65±.03	11.5±1.2	6.36±.22
$p_t = .3$	.40	.66±.01	8.02±.41	5.15±.19
	.50	.58±.03	8.95±1.04	4.50±.18
	.60	.60±.03	6.61±.85	4.34±.09
	.70	.63±.02	6.39±.38	4.29±.09
	.80	.59±.02	6.47±.51	4.35±.07
	.88	.50±.03	8.80±.91	4.94±.11
$p_t = .5$	.30	.66±.04	6.1 ±1.1	3.58±.15
	.50	.62±.03	3.36±.39	1.91±.06
	.80	.51±.02	3.14±.24	1.60±.03
$\pi^+ \to \pi^-$	.30	.70±.02	5.11±.47	3.52±.14
$p_t = .3$	.40	.64±.02	3.67±.34	2.02±.07
	.50	.59±.04	1.83±.25	1.11±.04
	.60	.67±.04	1.40±.20	0.97±.04
	.70	.66±.04	1.30±.18	0.83±.03
	.80	.65±.03	1.07±.13	0.65±.03
	.88	.54±.05	1.07±.20	0.46±.02
$p_t = .5$	.30	.63±.03	3.44±.38	1.76±.11
	.50	.64±.04	0.99±.16	0.67±.04
	.80	.57±.07	0.27±.07	0.14±.02
$\pi^+ \to K^+$	.30	.58±.08	1.49±.48	0.66±.12
$p_t = .3$	.40	.69±.06	0.72±.18	0.49±.08
	.50	.65±.05	0.61±.14	0.38±.07
	.60	.66±.07	0.40±.11	0.23±.03
	.70	.58±.07	0.45±.12	0.22±.03
$\pi^+ \to K^-$	.30	.70±.09	0.64±.24	0.40±.07
$p_t = .3$	.40	.64±.09	0.49±.16	0.33±.04
	.50	.63±.12	0.24±.11	0.16±.02
	.60	.76±.08	0.11±.03	.031±.014
	.70	.69±.10	0.12±.05	.068±.010
$\pi^+ \to p$	.30	.69±.06	1.27±.32	0.65±.07
$p_t = .3$	.40	.64±.04	0.93±.15	0.45±.06
	.50	.59±.05	0.63±.13	0.33±.05
	.60	.61±.09	.32±.12	0.17±.02
	.70	.59±.09	0.20±.06	0.11±.02
$p_t = .5$	.30	.75±.07	0.58±.16	0.43±.05
	.50	.66±.08	0.40±.12	0.19±.02

TABLE III (continued)

	x	α'	σ_0	σ_H
$p \to p$	.30	.61 ± .02	10.1 ± 1.0	5.62 ± .29
$p_t = .3$	.40	.59 ± .02	11.4 ± 0.8	6.41 ± .33
	.50	.55 ± .02	13.3 ± 1.2	8.51 ± .39
	.60	.51 ± .02	15.5 ± 1.2	10.00 ± .20
	.70	.49 ± .02	18.2 ± 1.5	10.72 ± .21
	.80	.51 ± .01	16.4 ± 0.8	11.75 ± .17
	.88	.46 ± .01	20.0 ± 1.0	13.60 ± .27
$p_t = .5$	.30	.60 ± .03	6.0 ± 0.8	2.90 ± .18
	.50	.50 ± .08	8.8 ± 2.7	3.79 ± .12
	.80	.46 ± .02	7.7 ± 0.7	4.14 ± .10
$p \to \pi^+$	.30	.58 ± .05	9.6 ± 2.0	5.50 ± .26
$p_t = .3$	.40	.56 ± .02	5.81 ± .51	2.34 ± .19
	.50	.54 ± .03	3.24 ± .38	1.78 ± .17
	.60	.59 ± .05	1.25 ± .26	0.81 ± .05
	.70	.56 ± .07	0.54 ± .14	0.37 ± .03
	.80	.60 ± .11	0.15 ± .07	.062 ± .014
$p_t = .5$	.30	.62 ± .04	3.94 ± .64	2.44 ± .16
	.50	.51 ± .11	1.62 ± .67	0.65 ± .04
$p \to \pi^-$	.30	.62 ± .04	4.28 ± .63	2.71 ± .16
$p_t = .3$	.40	.53 ± .06	2.60 ± .60	1.31 ± .07
	.50	.56 ± .12	0.72 ± .32	0.48 ± .04
	.60	.52 ± .08	0.41 ± .12	0.25 ± .02
	.70	.55 ± .13	0.09 ± .05	.077 ± .013
$p_t = .5$	.30	.55 ± .04	3.00 ± .51	1.33 ± .12
	.50	.43 ± .08	0.85 ± .25	0.23 ± .03

Note that when the cross-section *per nucleon* is parameterized as above, α is less than unity. When the *nuclear* cross-section is used instead, the slope becomes $\alpha' = 1 + \alpha$. Values of α' are listed in Table III. The variation of α' as a function of x is shown in Fig. 9 for various channels. Two extra points are also indicated along with the data. At $x = 0$ the value of α obtained from parametrizing the total absorption cross section is plotted [12]. At $x = 1$, a similar procedure was carried out. The probability to have only one collision in a nucleus (see Section 5) was parameterized as A^{α} and the resulting value of α was added to that obtained from the cross sections. The value of the sum was then plotted. Straight lines joining these two points are also shown. In the case of the $p \to p$ channel, the data for $x < 0.7$ are consistent with the line. For the $\pi^+ \to \pi^+$ data there appears to be a large deviation from the line in the x range of 0.65 to 0.8. This is just a reflection of the relative increase of resonance production from large A value targets previously described. From Fig. 9 it can be seen that a similar trend also exists in the $\pi^+ \to \pi^-$ channel.

5. *Comparison of experimental data with theoretical models*

The experimental data can be divided conveniently into two distinct classes. The higher statistics data (which consist mainly of the channels $\pi^+ \rightarrow \pi^+$ and $p \rightarrow p$) and the lower statistics data (for example $\pi^+ \rightarrow K^+$, $K^+ \rightarrow \pi^+$). The former set of data can be used to determine parameters in theoretical models whereas for the latter it is more appropriate to use models with definite input parameters. These two approaches will be considered in this section.

Higher statistics data

The specific channel $\pi^+Pb \rightarrow \pi^+X$ will be used for comparison with various general models. The experimental data is shown in Fig. 10 along with various predictions. The models that produced these predictions will now be dealt with in turn.

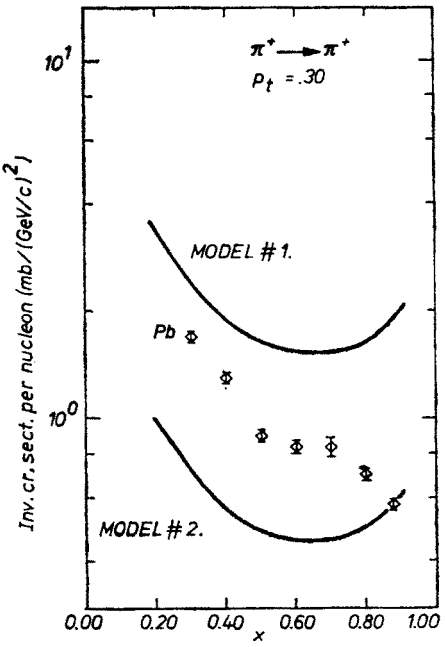

Fig. 10. The invariant differential cross section (data points) for the reaction $\pi^+Pb \rightarrow \pi^+X$. The two lines are predictions of models #1 and #2 mentioned in the text

Model #1

This model is shown pictorially in Fig. 11. The incident hadron, h, interacts with a nucleon situated in the upstream face of the nucleus. An hN interaction is assumed to take place with all the resulting secondaries emerging from the nucleus without further interaction. The probability of producing a specific secondary from a nucleus is related to the probability of producing the same particle from a nucleon by the ratio of the absorp-

tion cross sections, that is:

$$\left(E\frac{d^3\sigma}{dp^3}\right)_{hA} = \frac{\sigma^{hA}}{\sigma^{hN}}\left(E\frac{d^3\sigma}{dp^3}\right)_{hN}. \tag{10}$$

The factor σ^{hA}/σ^{hN} is a measure of the number of "front-face" nucleons that are available for an interaction with the incident hadron. Note that expression (10) is the probability

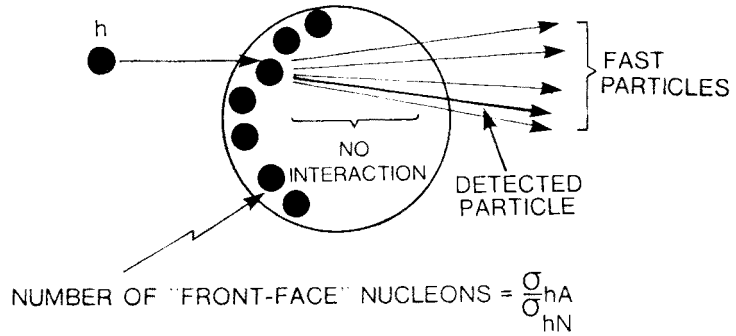

Fig. 11. Schematic diagram of model #1. A side view of the nucleus is shown with the incident hadron, h, coming in from the left

per nucleus. If this probability is rewritten as a probability *per nucleon*, expression (10) becomes:

$$\left(E\frac{d^3\sigma}{dp^3}\right)_{hA} = \frac{1}{\bar{\nu}}\left(E\frac{d^3\sigma}{dp^3}\right)_{hN}. \tag{11}$$

This model therefore predicts the same x-dependence for the hA cross section as the hN cross section; only a shift in magnitude will take place. From Fig. 10 it is evident that this model is in serious disagreement with the experimental data, being at least a factor of 2 larger than the data in the range $x \gtrsim 0.5$.

Model #2

Model #2 issumes the opposite extreme situation to Model #1. Rather than having all the secondaries escape without further interaction, here it is assumed that *all* the products of an hN interaction in the upstream face of the nucleus are absorbed if they are involved in further collisions with subsequent nucleons. Consequently, only secondaries that are produced by interactions that take place in the periphery of the nucleus (see Fig. 12) will emerge from the interaction. The probability of the incident hadron having one and only one collision in the nucleus can be calculated using a multiple-scattering model. The result is [5]:

$$p(1) = \int_{-\infty}^{\infty} (\sigma^{hN}l)e^{-\sigma^{hN}l}d^2b. \tag{12}$$

σ^{hN} is the hN total absorption cross section, l is the thickness of the nucleus at an impact parameter b. It should be noted that the expression for $p(1)$ was derived assuming that the

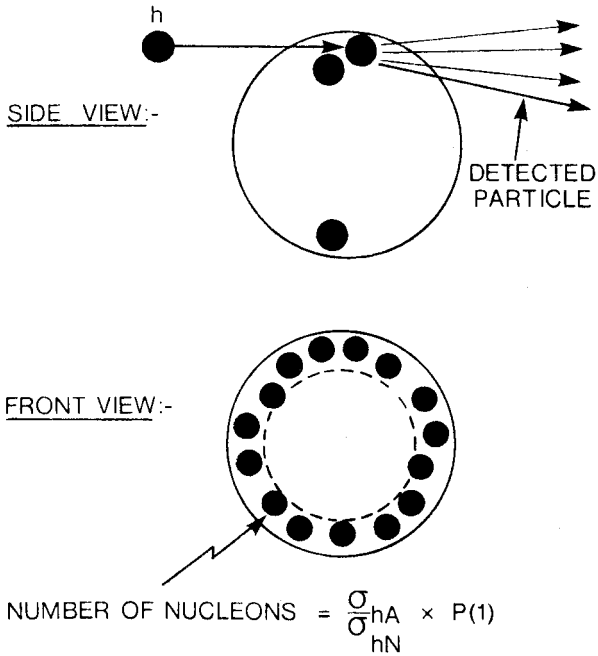

Fig. 12. Schematic diagram of model #2. Side and front views of the nucleus are shown with the incident hadron entering from the left

probability for subsequent interactions in the nucleus is governed by σ^{hN}. This was also assumed in the derivation of $\bar{\nu}$.

The hA and hN differential cross sections are therefore related in this model by:

$$\left(E\frac{d^3\sigma}{dp^3}\right)_{hA} = \frac{p(1)}{\bar{\nu}}\left(E\frac{d^3\sigma}{dp^3}\right)_{hN}. \tag{13}$$

Again, the x-dependence for hA and hN interactions is predicted to be the same. As shown in Fig. 10 this disagrees with the data. However, there is good agreement between the data

TABLE IV

Comparison of measured cross sections (at $x = 0.88$) and predictions from Model #2 for production from a lead target. R is the predicted cross section divided by the measured cross section

Channel	R
$\pi^+ \to \pi^+$	0.91 ± 0.03
$K^+ \to K^+$	1.02 ± 0.19
$p \to p$	0.77 ± 0.03
$\pi^+ \to K^+$	0.56 ± 0.09
$\pi^+ \to \pi^-$	0.62 ± 0.07
$p \to \pi^+$	0.12 ± 0.11

and this model at high x. This is also apparent from Fig. 9 where the values of α' at high x are consistent with a single scattering having taken place in the nucleus.

Comparisons of the measured cross sections for various channels and theoretical predictions from expression (13) are listed in Table IV. From the good agreement it can be concluded that the high momentum particles ($x \gtrsim 0.9$) that are produced in hA interactions where the incident and final particles are identical are formed in a single "hN-like" collision that typically take place in the skin-depth of the nucleus.

Model #3

From Fig. 10 it can be seen that the experimental data lie in between the two extremes described by the two previous models. Probably a more realistic approach is to assume that the state formed in the first hN collision propagates in some manner through the nucleus. This approach is the basis of Model #3 which is summarized schematically in Fig. 13. The incident hadron interacts with a nucleon in the upstream face of the nucleus. The main result of this interaction is a state with a large fraction (x_1) of the incident momentum p_{inc}. There are also low momentum particles formed but these do not effect the predictions of this model as only high momentum secondaries are being considered. The high momentum state then interacts again with subsequent nucleons. In order to make predictions, it is assumed that this state has the same total absorption cross section as the incident hadron. After undergoing several collisions, $\nu-1$ in all, the momentum of the hadronic state is degraded. The state then interacts finally with a nucleon situated near

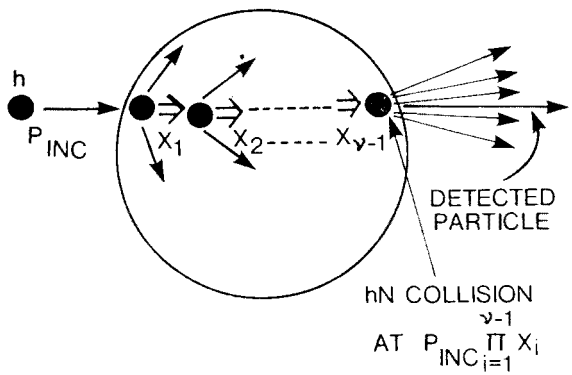

Fig. 13. Schematic diagram of model #3. A side view of the nucleus is shown with the incident hadron entering from the left

the downstream face of the nucleus. It is assumed that a "hN-like" collision occurs from which the detected particles are formed. There are, therefore, ν collisions in all. The total number of collisions that the hadronic state undergoes can be calculated using a multiple scattering model. The probability of ν collisions is:

$$p(\nu) = \frac{1}{\nu!} \int_{-\infty}^{\infty} (\sigma^{hN_i})^{\nu} e^{-\sigma^{hN_i}} d^2b. \tag{14}$$

Typical values of $p(\nu)$ are shown in Fig. 14.

In summary, this model is a multiple-scattering model in which $\nu-1$ collisions occur before a "hN-like" interaction takes place. The incident momentum for this hN interaction is $(\prod_{i=1}^{\nu-1} x_i)p_{\text{inc}}$.

One now has the freedom to choose the value of x that occurs after each collision up to the penultimate one. Various choices will now be considered.

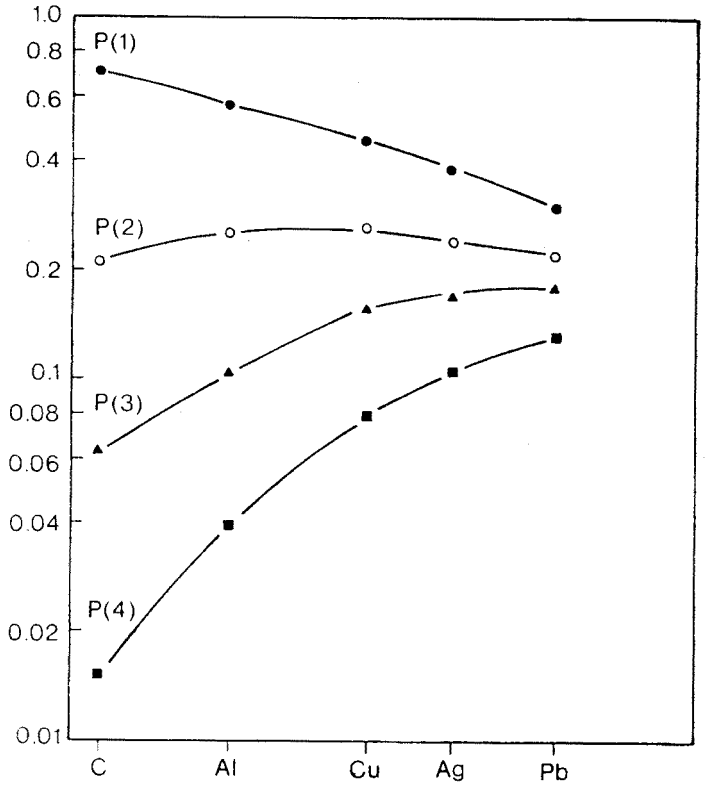

Fig. 14. Probability of a π^+ to have ν collisions in a nucleus as a function of A, the atomic number

(A) A natural choice for the x probability distribution, $P(x)$, would be the measured hN differential cross section. This is equivalent to assuming that the hadronic state formed after an hN collision has the same momentum as a single hadron formed in a similar interaction. The predictions of such an assumption are shown in Fig. 15(a). It is evident that there is a large disagreement with the experimental data. In fact, the predictions of this model are very similar to those of Model #2. This is not surprising! Most interactions involving more than one collision will produce particles with momentum below that measured in this experiment (from Fig. 5 it can be seen that the mean value of x for a π^+ produced in a $\pi^+p \to \pi^+X$ interaction is approximately 0.5. For two successive collisions this value dropped to ~ 0.2). Therefore, only interactions involving one hN collision will produce particles with $x \gtrsim 0.3$. This was precisely the basis of Model #2.

(B) A less extreme assumption for $P(x)$ obviously has to be made. Rather than assume $P(x)$ is similar to that measured in hN interactions, one can assume it is a delta function. Constraining x to be $= 1$ for the first $\nu-1$ collisions will just lead to the same results predicted by Model #1. To compromise, constant x values ranging from 0.7 to 0.95 were assumed for all collisions except of course the last one which will still be "hN-like". The

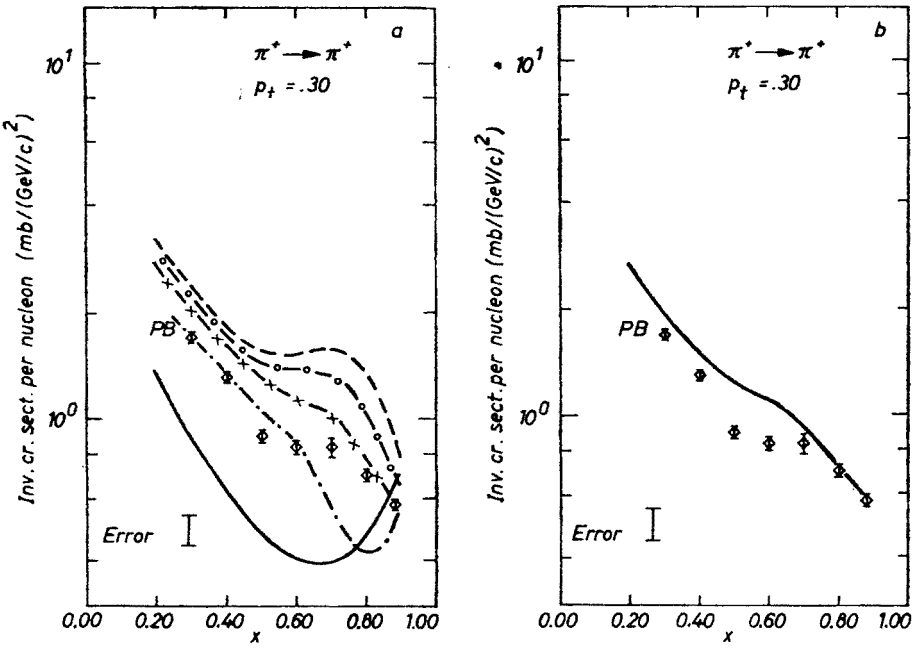

Fig. 15. (a) Theoretical predictions for the channel π^+Pb $\rightarrow \pi^+$X. The dashed line is the result of assuming $x = 0.95$ for the flux; the dashed-circle line assumes $x = 0.9$; the dashed-crossed line assumes $x = 0.85$ and the dashed-dotted line assumes $x = 0.7$. The solid line is the result of assuming that a "hN-like" interaction occurs at each collision. The typical error on the predictions is also indicated. (b) Theoretical predictions for the channel π^+Pb $\rightarrow \pi^+$X. The solid line is a theoretical prediction that results from assuming that $x = 0.9$ for the flux after each collision and a transverse momentum kick distributed as for hN interactions occurs. A typical error on the prediction is also indicated

reasons for choosing such values of x were not arbitrary. The idea of a hadronic state (or flux) existing immediately after an hN collision has been extensively formulated by Gottfried [13]. In his model, the fraction of incident momentum, p, that the flux has after one collision is $1-p^{-2/3}$, where p is measured in GeV/c. In the 50 $\rightarrow$ 100 GeV/c range this fraction is between 0.93 and 0.95.

A similar approach has been used to analyze massive dimuon production [14]. Once again, it has been concluded that the flux has to carry at least 90% of the incident momentum.

The results of assuming a constant value for x are shown in Fig. 15(a). For the first time the predicted hA cross section has an x-variation that differs significantly from the hN cross section.

(C) One last refinement can be made to this model. To obtain the previous prediction (Model #3(B)), it was assumed that the transverse momentum of the detected particle resulted solely from the final collision in the nucleus. All interactions other than the last one (the "hN-like" collision) contributed no transverse momentum. An alternative

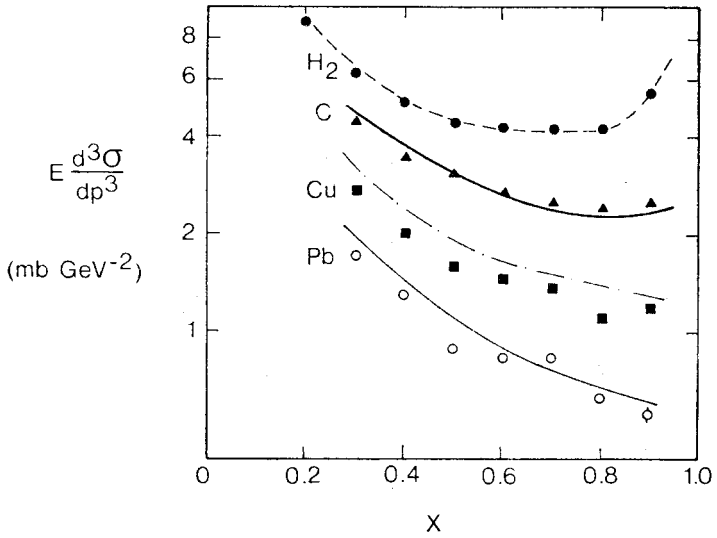

Fig. 16. Comparison between theoretical predictions (lines) from model #3(C) and experimental data (points) for the reaction channel $\pi^+A \rightarrow \pi^+X$ where A, the nuclear target is C, Cu or Pb

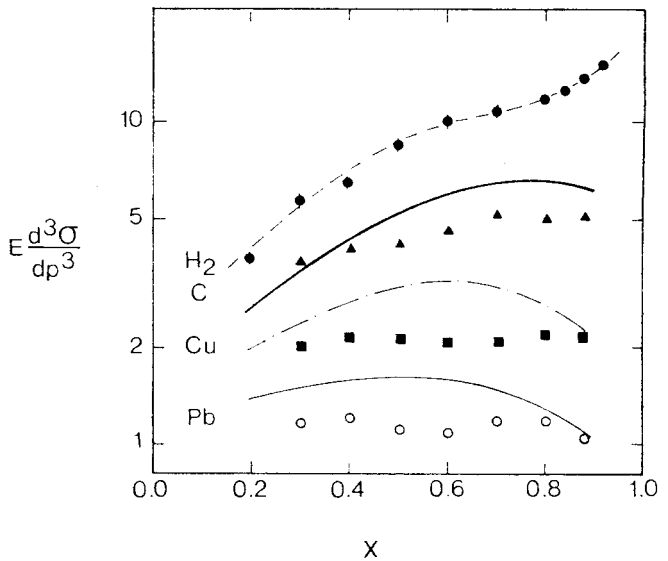

Fig. 17. Comparison between theoretical predictions (lines) from model #3(C) and experimental data (points) for the reaction channel $pA \rightarrow pX$ where A, the nuclear target, is C, Cu or Pb

approach is to assume a true multiple-scattering process where, after every collision, the hadronic state receives a transverse momentum "kick". The size of this "kick" is assumed to be distributed as in a hN interaction. The prediction of this final model is shown in Fig. 15(b).

To test the validity of this type of approach, predictions for nuclei ranging from C to Pb are shown in Figs. 16 and 17 for data from the leading channels $\pi^+ \to \pi^+$ and $p \to p$.

In conclusion, there appears to be evidence favouring a multiple-scattering picture for hA interactions when the final particle is the same as the incident particle. An independent method of testing this hypothesis is to examine the dependence of the hA cross section on transverse momentum. If the hadronic state undergoes ν collisions without significant change of the momentum, one would naively expect the p_t distribution to widen by a factor of $\sqrt{\bar{\nu}}$. A more sensitive test is to compare the slope of the p_t distribution. In this case it should differ by a factor of $1/\nu$ when hA data is compared to hN data.

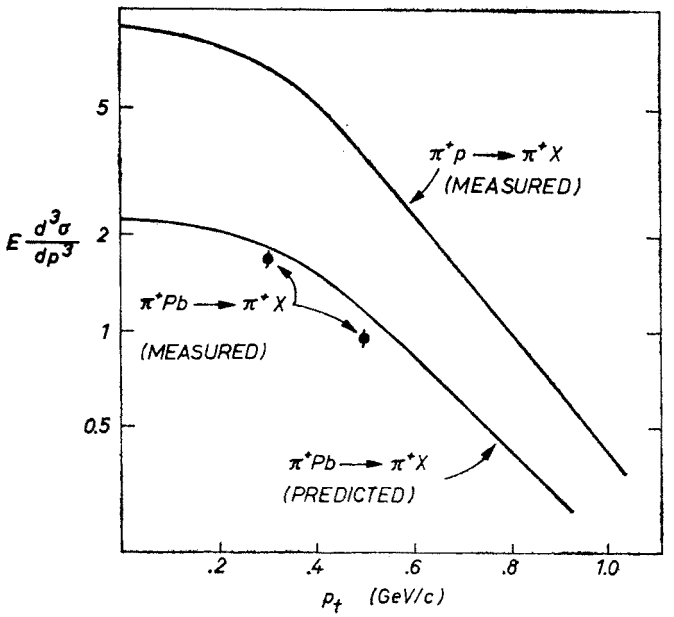

Fig. 18. Variations of invariant differential cross section with transverse momentum. The experimental data (points) and the theoretical predictions from model #3(C) (lines) are for an x value of 0.3. Hydrogen data (Ref. [8]) is also shown for comparison

A comparison of experimental data and theoretical prediction is shown in Fig. 18. The data is consistent with the model. Notice that the slope of the hA cross section in the region of $p_t = 0.4$ GeV/c is approximately equal with that of the hN cross section. This would seem to contradict the above reasoning which would appear to predict a difference of a factor of ~ 2.8, the value of $\bar{\nu}$ for π^+ incident on a lead target. However, it is the shape of the $p(\nu)$ distribution that is important.

Lower statistics data

Many models [15] have been proposed to explain the nondiffractive production of hadrons with large x and small p_t from hydrogen. Recently attempts have been made [16] to extend these ideas to production from nuclear targets. A summary of some of the ideas behind these models will be given here. The channels $\pi^+ \to K^+$ and $K^+ \to \pi^+$ will be used for illustration. For both channels the common valence quark in the incident and final particles is a u quark. It is assumed that the common quark is in fact transmitted through the nucleus without scattering. The other valence quark in the incident hadron is absorbed by the nucleus. The probability, P, for this to occur can be written as:

$$P = \frac{1}{\sigma^{\pi A}} \int_{-\infty}^{\infty} [1 - e^{-\sigma^{\bar{q}N} l}] e^{-\sigma^{uN} l} d^2b \tag{15}$$

for the channel $\pi^+ \to K^+$. Note that the absorbed quark is a $\bar{d}$ quark whereas for the channel $K^+ \to \pi^+$ it is an $\bar{s}$ quark. Using equation (15) leads to the following prediction for the hA cross section [16c]:

$$\left(E\frac{d^3\sigma}{dp^3}\right)_{hA\to h'X} = \left(\frac{\sigma^{hA} - \sigma^{qA}}{\sigma^{hN} - \sigma^{qN}}\right)\left(E\frac{d^3\sigma}{dp^3}\right)_{hN\to h'X} \tag{16}$$

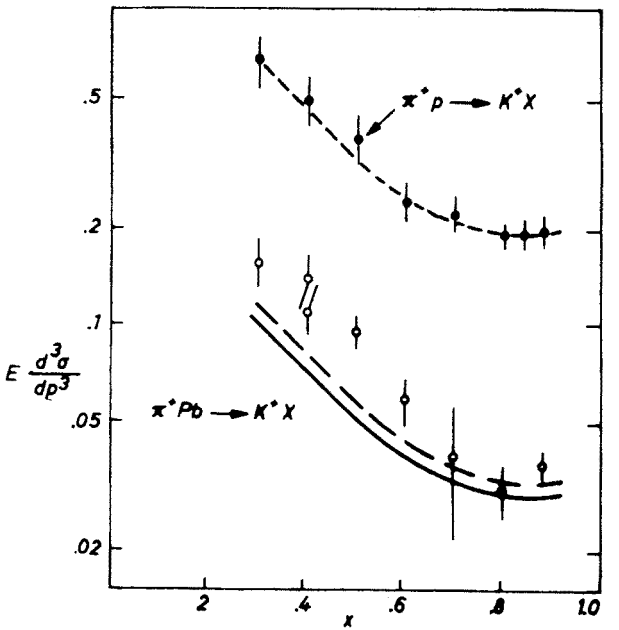

Fig. 19. Comparison between theoretical predictions, Refs. [16a] and [16c], (lines) and experimental data (points) for the reaction $\pi^+Pb \to K^+X$ measured at $p_t = 0.3$ GeV/c. Data from a hydrogen target (Ref. [8]) are shown for comparison. The dashed line drawn through the hydrogen data was used as input to the 2 theoretical models

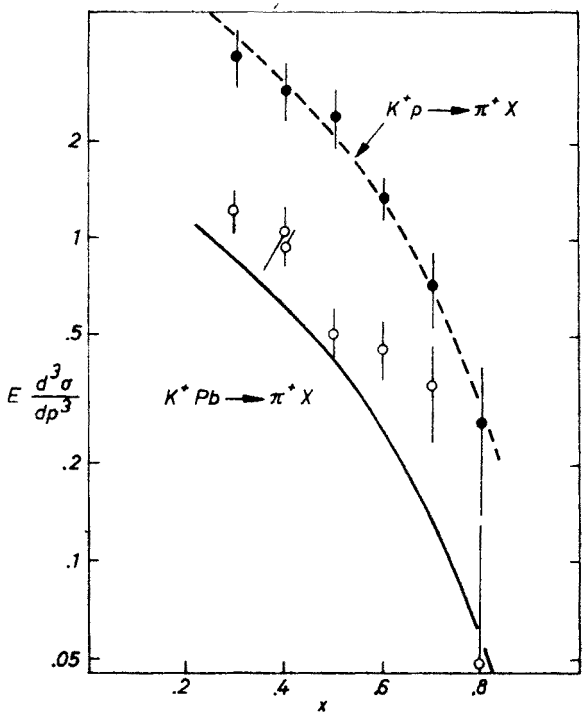

Fig. 20. Comparison between theoretical predictions, Ref. [16c] (lines) and experimental data (points) for the reaction $K^+Pb \rightarrow \pi^+X$ measured at $p_t = 0.3$ GeV/c. Data from a hydrogen target (Ref. [8]) are shown for comparison. The continuous line drawn through the hydrogen data was used as input to the theoretical model

(q is the transmitted quark. σ^{qA} can be estimated by using the model described by expression (14). In this case, of course, the quark–nucleon cross section σ^{qN} has to be used. This was estimated by using the additive-quark-model relations [17]. Note that equation 16 predicts an A dependence that does not vary with x. This is consistent with the variation of α' shown in Fig. 9 for the channel $\pi^+ \rightarrow K^+$. The predictions of this model are shown in Figs. 19 and 20. The overall agreement is encouraging.

6. *Conclusions*

The following conclusions can be drawn concerning the new data from FNAL experiment #451.

(1) Differences exist when nuclear target data are compared to data from hydrogen. Production of all high momentum secondaries is suppressed regardless of the incident particle type. When the produced particle is the same as the incident one, the A dependence of the nuclear cross section is significantly different from the hydrogen cross section.

(2) Similarities between the nuclear and hydrogen data are evident when *relative* production rates are compared.

(3) The production of very high momentum secondaries ($x \gtrsim 0.9$) in reactions where the incident and final particles are the same, is due to single "hN-like" collisions in the nucleus.

(4) The higher statistics data (for example, p → p) agrees with the idea that a hadronic "flux" travels through the nucleus with its momentum being degraded at each collision with a nucleon.

(5) The lower statistics data (e.g. $\pi^+ \to K^+$, $K^+ \to \pi^+$) are consistent with theoretical models that assume quark absorption in the nucleus.

(6) The p_t data is too sparse to determine the extent of multiple scattering in the nucleus.

I received much guidance through extensive discussions with J. Nassalski (Institute of Nuclear Research, Warsaw, Poland) in the course of preparing this document. This work was supported in part by the U.S. Department of Energy, the National Science Special Foreign Currency Program and the Istituto Nazionale di Fisica Nucleare, Italy.

Editorial note. This article was proofread by the editors only, not by the author.

REFERENCES

[1] For recent experimental reviews on various aspects of hadron-nucleus interactions see I. Otterlund, *Acta Phys. Pol.* **B8**, 119 (1977); W. Busza, *Acta Phys. Pol.* **B8**, 333 (1977); C. Halliwell, in proceedings of the Eighth International Symposium on Multiparticle Dynamics, Kayserberg, 1977, edited by R. Arnold et al., Centre de Recherches Nucleaires, Strasbourg, France 1977.

[2] J. E. Elias et al., *Phys. Rev. Lett.* **41**, 285 (1978).

[3] S. A. Azimov et al. in *Multiparticle Production on Nuclei at Very High Energies*, edited by G. Bellini et al., ICTP, Trieste 1977; E. G. Boos et al., *Nucl. Phys.* **B143**, 232 (1978); D. Chaney et al., *Phys. Rev.* **D19**, 3210 (1979).

[4] J. E. Elias et al., (to be published in Phys. Rev. D)

[5] A further understanding of $\bar{\nu}$ and the probability of a hadron multiply scattering within a nucleus can be gained from Ref. [4].

[6] Details of this experiment can be found in the preprint A. E. Brenner et al., Fermilab-Conf-80/47-Exp.

[7] The ratio $|\vec{p}'|/|\vec{p}|$ was defined as x. For the kinematic range of this experiment, this variable is extremely close to the Feynman x variable.

[8] W. W. Toy, Ph. D. thesis, M.I.T., 1978 (unpublished); W. Aitkenhead, Ph.D. thesis, M.I.T., 1979 (unpublished); D. Cutts et al., *Phys. Rev. Lett.* **43**, 319 (1979).

[9] T. Eichten et al., *Nucl. Phys.* **B44**, 333 (1972); K. Heller et al., *Phys. Rev.* **D16**, 2737 (1977); M. R. Whalley et al., Univ. of Michigan Report Um-He 79-14.

[10] D. Cutts et al., *Phys. Rev. Lett.* **40**, 141 (1978).

[11] For example, S. P. Denisov et al., *Nucl. Phys.* **B61**, 62 (1973).

[12] The values of 0.762, 0.782 and 0.719 were obtained for incident π^+, K^+ and p from A. S. Carroll et al., *Phys. Lett.* **80B**, 319 (1979).

[13] K. Gottfried, *Phys. Rev. Lett.* **32**, 957 (1974).

[14] T. Jaroszewicz, M. Jeżabek, *Z. Phys.* **C4**, 277 (1980).

[15] For example, K. P. Das, R. C. Hwa, R. C. Hwa, *Phys. Lett.* **68B**, 459 (1977); D. W. Duke, F. E. Taylor, *Phys. Rev.* **D17**, 1788 (1978).

[16] For example, a) V. V. Anisovich et al., *Nucl. Phys.* **B133**, 477 (1978); b) A. Białas, Fermilab Report, Fermilab-Conf-79/35-THY; c) A. Dar, F. Takagi, *Phys. Rev. Lett.* **44**, 768 (1980).

[17] The relations $\sigma^{uN} = \sigma^{\bar{u}N} = \sigma^{dN} = \sigma^{\bar{d}N} = \frac{1}{2}\sigma^{\pi N}$ and $\sigma^{sN} = \sigma^{\bar{s}N} = \sigma^{KN} - \frac{1}{2}\sigma^{\pi N}$ were used.